What is Tide-Induced Residual Current?

NORIHISA IMASATO

Geophysical Institute, Kyoto University, Kyoto 606 Japan

1 October 1982 and 24 February 1983

ABSTRACT

We carried out a numerical experiment to study the velocity field of a two-dimensional tidal current in a simple model basin with a narrow strait. It was found that the tide-induced transient eddy (TITE) originated from the low pressure area that is generated downstream behind a headland by the nonlinearity or the centrifugal force of the tidal current flowing with a large curvature through a narrow channel. The transient eddy is maintained during certain phases of the tide, and therefore the Eulerian tide-induced residual current is the result of the averaging process of transient phenomena; the Eulerian residual current is only a mathematical representation of the tide-induced transient eddy and has no physical reality. We should abandon the concept of residual velocity.

The lifetime of TITE depends on the magnitude of vorticity and its dissipation. In an inner basin with large bottom friction, the eddy diminishes within a short time (one or two hours) after the generation, and the pressure gradient of the eddy is smaller than the pressure gradient of tidal flow in the strait at the time of high-tide slack water. In this case, TITE is swept away by the ebbing tidal current which flows outward through the strait and soon disappears. On the other hand, in a basin with small bottom friction, because the eddy grows so strong at the time of the start of the ebb tide that the pressure gradient becomes larger than that of the ebbing tide, it is maintained by the ebbing tidal current which runs around the eddy toward the strait. In the latter case, vorticity dissipation caused by horizontal eddy viscosity is larger than that due to bottom friction because of a large horizontal velocity shear near the eddy.

1. Introduction

It has been reported that tide-induced residual circulations are induced in an inner basin with a narrow channel by the nonlinearity of the tidal current flowing through the channel (Tee, 1976; Yanagi, 1976, 1978; Oonishi, 1977). Two-dimensional Eulerian residual velocity $\mathbf{U}_C(x, y)$ in a basin with a constant depth H is related to two-dimensional Eulerian residual transport velocity $\mathbf{U}_{CT}(x, y)$ (Cheng and Casulli, 1982):

$$\mathbf{U}_{CT}(x, y) = \frac{\langle [H + \eta(x, y, t)]\mathbf{U}(x, y, t)\rangle}{H} = \mathbf{U}_C(x, y) + \frac{\langle \eta \mathbf{U}\rangle}{H}, \quad (1a)$$

$$\mathbf{U}(x, y, t) = \mathbf{U}_T(x, y, t) + \mathbf{U}_C(x, y), \quad (1b)$$

where x and y are the Cartesian coordinates in the horizontal plane, t is time, $\eta(x, y, t)$ is the free-surface displacement measured from mean sea level with the positive direction of z pointing upward, $\mathbf{U}(x, y, t)$ is the current velocity including the periodic tidal velocity $\mathbf{U}_T(x, y, t)$ and the Eulerian tide-induced residual velocity $\mathbf{U}_C(x, y)$; angle brackets denote time average of a variable over a tidal period.

Tee (1976) called $\mathbf{U}_{CT}$ the Lagrangian residual velocity, but Zimmerman (1979) and Cheng and Casulli (1982) showed that $\mathbf{U}_{CT}$ is not a Lagrangian variable and should be called the Eulerian residual transport velocity. In previous studies on the Eulerian residual circulation, Eulerian tide-induced residual current (TIRC) is considered to be a time-independent or steady current, or a current with a time scale much longer than a tidal period. However, in this paper we concluded that the residual current has no physical reality and we should abandon the concept of the residual velocity. Because $\mathbf{U}_{CT}$ differs by only 2–3% from $\mathbf{U}_C$ in this investigation and also because the primary objective is determination of the time-dependence or physical reality of the Eulerian residual current, we consider mainly the Eulerian tide-induced residual velocity $\mathbf{U}_C$ and only briefly discuss the Eulerian residual transport velocity $\mathbf{U}_{CT}$.

Nonlinear tidal current ($\mathbf{U}_T$) flows into an inner basin through a narrow channel and generates another current [$\mathbf{U}_N(x, y, t)$]. However, $\mathbf{U}_N$ is not equal to the Eulerian residual velocity $\mathbf{U}_C$ but it is associated with the transient eddy which is generated downstream behind a headland during certain phases of the tide, and it has the same time scale as that of the tidal current ($\mathbf{U}_T$) which is the external forcing factor. As a result, the Eulerian tide-induced residual current is only a mathematical description of the transient eddy ($\mathbf{U}_N$) and has no physical reality because it is the result of the averaging process of transient phenomena. Thus, we carried out a numerical experiment to

confirm this speculation and also to clarify the characteristics of the transient eddy $\mathbf{U}_N$.

2. Numerical model

The equations governing the vertically averaged two-dimensional tidal current are

$$\frac{\partial \mathbf{U}}{\partial t} + \mathbf{U}\cdot\nabla_H\mathbf{U} + f(\mathbf{k}\times\mathbf{U}) = -g\nabla_H\eta + \nu_H\nabla^{H2}\mathbf{U} + \tau, \quad (2)$$

$$\frac{\partial \eta}{\partial t} = -\nabla_H[(H+\eta)\mathbf{U}], \quad (3)$$

where we have assumed a hydrostatic balance in a homogeneous fluid. The operator ∇_H is $i\frac{\partial}{\partial x} + j\times\frac{\partial}{\partial y}$ and $\nabla_H{}^2$ is $\frac{\partial^2}{\partial x^2}+\frac{\partial^2}{\partial y^2}$. The $\mathbf{U}$ is the vertically averaged horizontal velocity vector with components U and V in the Eulerian system of coordinates x and y, η the height of water surface above the mean sea level, H (30 m) the depth of the uniform bottom, f (7.7×10^{-5} s^{-1}) the Coriolis parameter, g (980 cm s^{-2}) the acceleration of gravity, $\mathbf{k}$ the unit vector pointing positive upward, and ν_H (5.5×10^5 cm^2 s^{-1}) the constant horizontal eddy viscosity. In (2) τ is the bottom friction vector with components τ_x and τ_y in the x and y direction, respectively, and it is assumed to be represented by a quadratic term with coefficient $\gamma_b{}^2$,

$$\tau = (\tau_x, \tau_y) = -\gamma_b{}^2\mathbf{U}|\mathbf{U}|(H+\eta)^{-1}. \quad (4)$$

We use the simple basin model shown in Fig. 1. In this model, the inner basin (55 km × 20 km) is connected with the outer basin by the channel (8 km × 3 km). The calculated area is divided into square meshes with a grid size of 0.5 km × 0.5 km. Therefore, the resolution of this grid system is suitable for depicting the velocity shear of the tidal current near the channel. The barotropic water motion is derived from the tidal elevation which is given along the open boundary (dashed line in Fig. 1) by Eq. (5),

$$\eta = \eta_0\cdot\sin(2\pi t/T), \quad (5)$$

where η_0 and T are the amplitude and the period of the M_2 tide, respectively. The initial values of U, V and η are zero in the whole basin. After integrating Eqs. (2) and (3) by the ADI method (Leendertse, 1971) for five cycles of the M_2 tide, we have a stationary state of the M_2 tide; a time step of 22.5 lunar seconds is used in the present model.

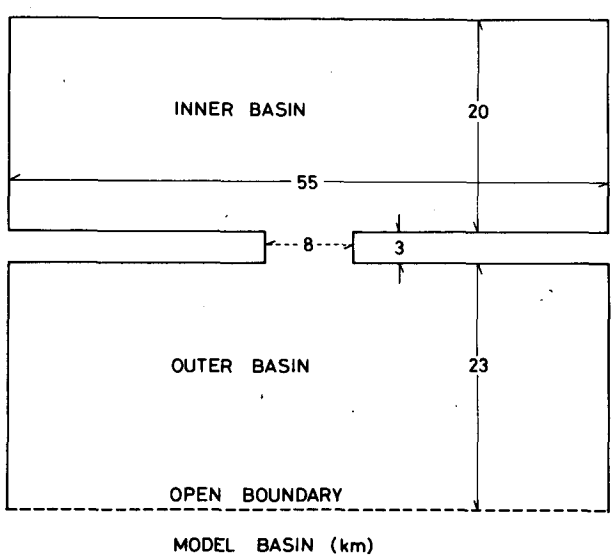

FIG. 1. Model basin.

3. Defining Eulerian tide-induced residual current

Next, we calculated the velocity field under the conditions of $\gamma_b{}^2 = 2.6\times10^{-3}$ (Hansen, 1956) and $\eta_0 = 100$ cm; this calculation is designated Case I. Fig. 2 shows the calculated velocity fields near the strait during flood current. Panel D of Fig. 2 illustrates that circular currents are generated in the downstream area (in the inner basin) behind the headlands, but in the upstream area (in the outer basin) tidal current flows almost as a potential flow and generates no circular current. Panels C–E show that a small circulation is generated behind the headlands, becomes a large eddy and then disappears soon after the beginning of ebb tide. Figure 3 depicts the calculated velocity field of the Eulerian tide-induced residual current (TIRC) $\mathbf{U}_C$ defined by Eq. (6) from previous studies on TIRC,

$$\mathbf{U}_C(x,y) = \frac{1}{T}\int_0^T \mathbf{U}(x,y,t)dt. \quad (6)$$

Four circulations of TIRC can be seen; the maximum speed is 26 cm s^{-1} near the strait. Two of these circulations exist in the inner basin; the others in the outer basin. Panel E in Fig. 2 shows the velocity field at the time of high-tide slack water. Although the two circulations in the inner basin are similar to the circulations of TIRC in Fig. 3, no circulation can be found in the outer basin. The velocity field in this panel confirms that TIRC is not a time-independent flow because, if Eq. (1) is correct for the velocity field of a nonlinear tidal current near the strait, then the velocity vectors in Fig. 2E should represent those of $\mathbf{U}_C$. Thus, we conclude that the so-called TIRC as defined by Eq. (6) is only a mathematical result produced by the time-average of the transient circulation over the tidal period and is not a physical entity. Also, the previous theory concerning TIRC is not appli-

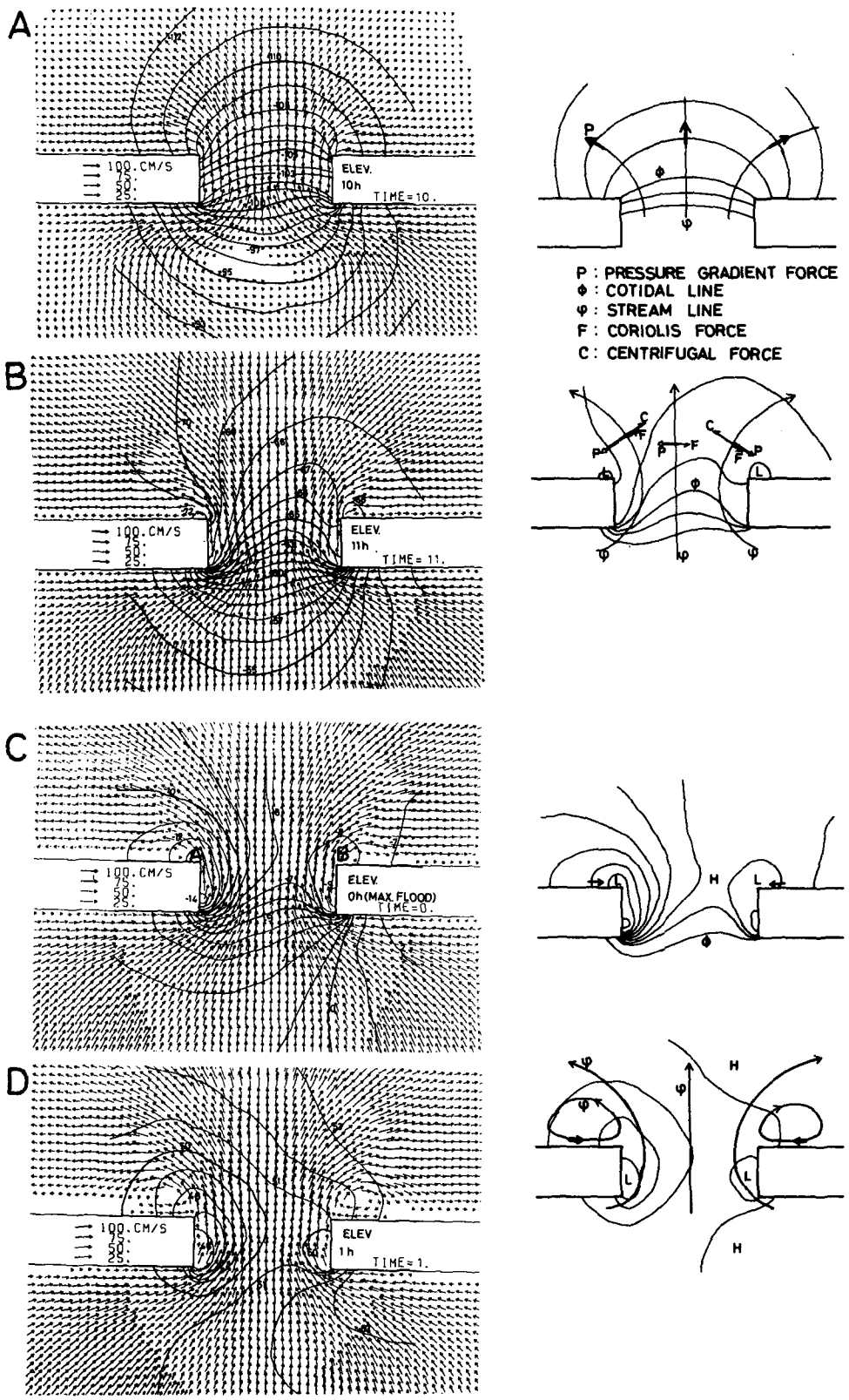

FIG. 2. Distribution of velocity vectors of tidal current in Case I: (A) 10 h (one hour after the time of low-tide slack water), (B) 11 h, (C) 0 h (the time of maximum flood current), (D) 1 h and (E) 3 h (just before the time of high-tide slack water). Right panels show the schematic diagram.

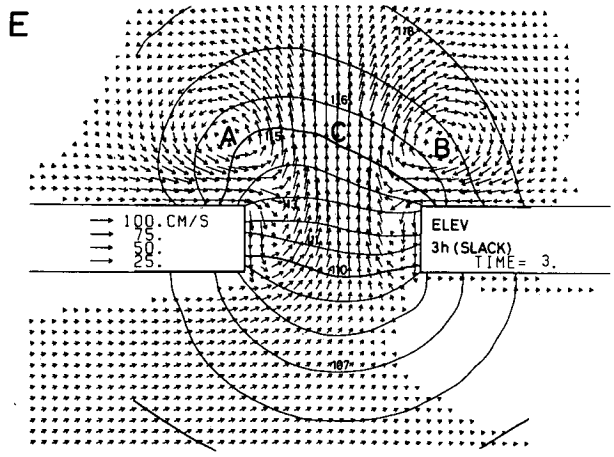

FIG. 2. (*Continued*)

cable for explaining the phenomena occurring near a strait.

Therefore, we should define the velocity field as:

$$\mathbf{U}(x, y, t) = \mathbf{U}_T(x, y, t) + \mathbf{U}_N(x, y, t) = \mathbf{U}_T(x, y, t) + \sum_{i=0}^{\infty} \mathbf{U}_N^i(x, y) \cdot \exp(j \cdot 2\pi t/T_i), \quad (7)$$

where j is $\sqrt{-1}$, $\mathbf{U}_T$ denotes the velocity of a tidal current as a potential flow, $\mathbf{U}_N$ the velocity of the transient circular currents induced behind a headland, and $\mathbf{U}_N^i$ and T_i denote the amplitude and the period of the ith constituent of $\mathbf{U}_N$, respectively. Therefore in this paper, we call the transient circular current the "tide-induced transient eddy (TITE)" and we will discuss some of the characteristics of TITE in the following sections.

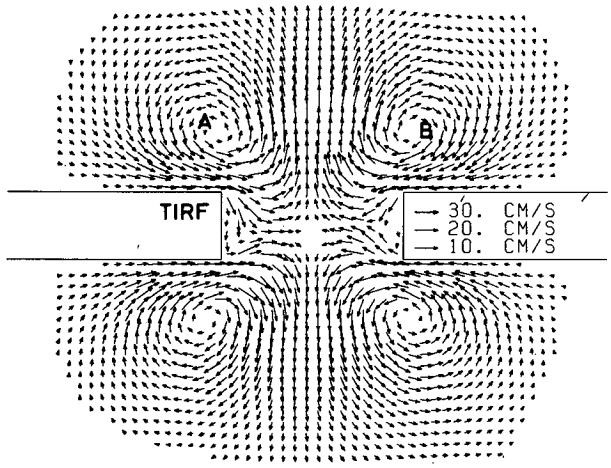

FIG. 3. Distribution of velocity vectors of TIRC in Case I. Symbols A and B show the center of transient eddies in Fig. 2E.

TABLE 1. Parameters of Cases I–IV.

Case	η_0 (cm)	γ_b^2	ν_H (cm^2 s^{-1})	Lifetime of TITE (h)
I	100	2.6×10^{-3}	5.5×10^5	3–4
II	200	2.6×10^{-3}	5.5×10^5	4–5
III	200	1.04×10^{-3}	5.5×10^5	7–8
IV	200	0.26×10^{-3}	5.5×10^5	10–11

4. The mechanism of generation of the tide-induced transient eddy (TITE)

Next, we turn our attention to the mechanism of generation of TITE induced transiently behind a cape of a peninsula in a flood tide. In Fig. 2, the solid curves give water surface elevation at intervals of 1 cm, and they also show the isobaric contours. Moreover, the schematic diagrams on the right side of Fig. 2 show the relation between an instantaneous streamline ψ and an isobaric curve Φ, and also the relation among three vectors of the pressure gradient force P, the centrifugal force C and Coriolis force F. In Fig. 2A, the velocity vectors and the isobaric curves intersect each other almost perpendicularly near the strait; i.e., after the beginning of flood tide, water is driven directly by the pressure gradient force induced by the tide of an external force. During flood tide, water enters into the inner basin through the strait with a large curvature. Therefore, in the western area of the strait the pressure gradient force P is balanced

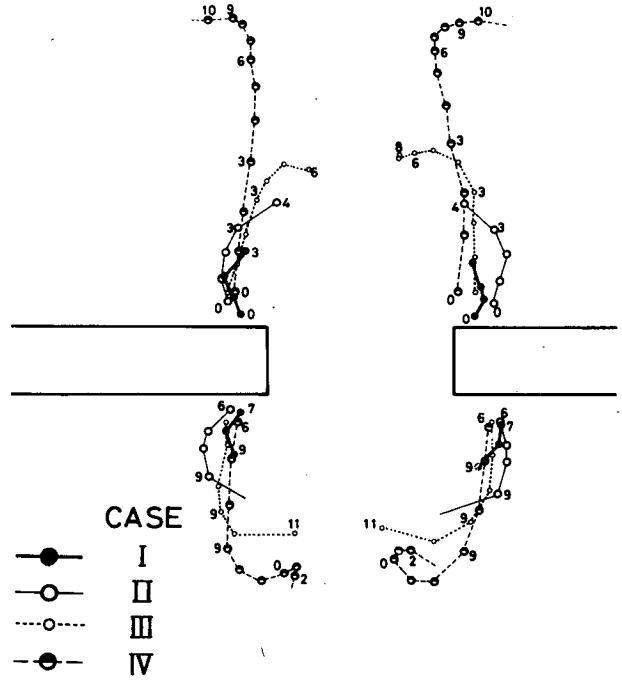

FIG. 4. Loci of center of tide-induced transient eddies.

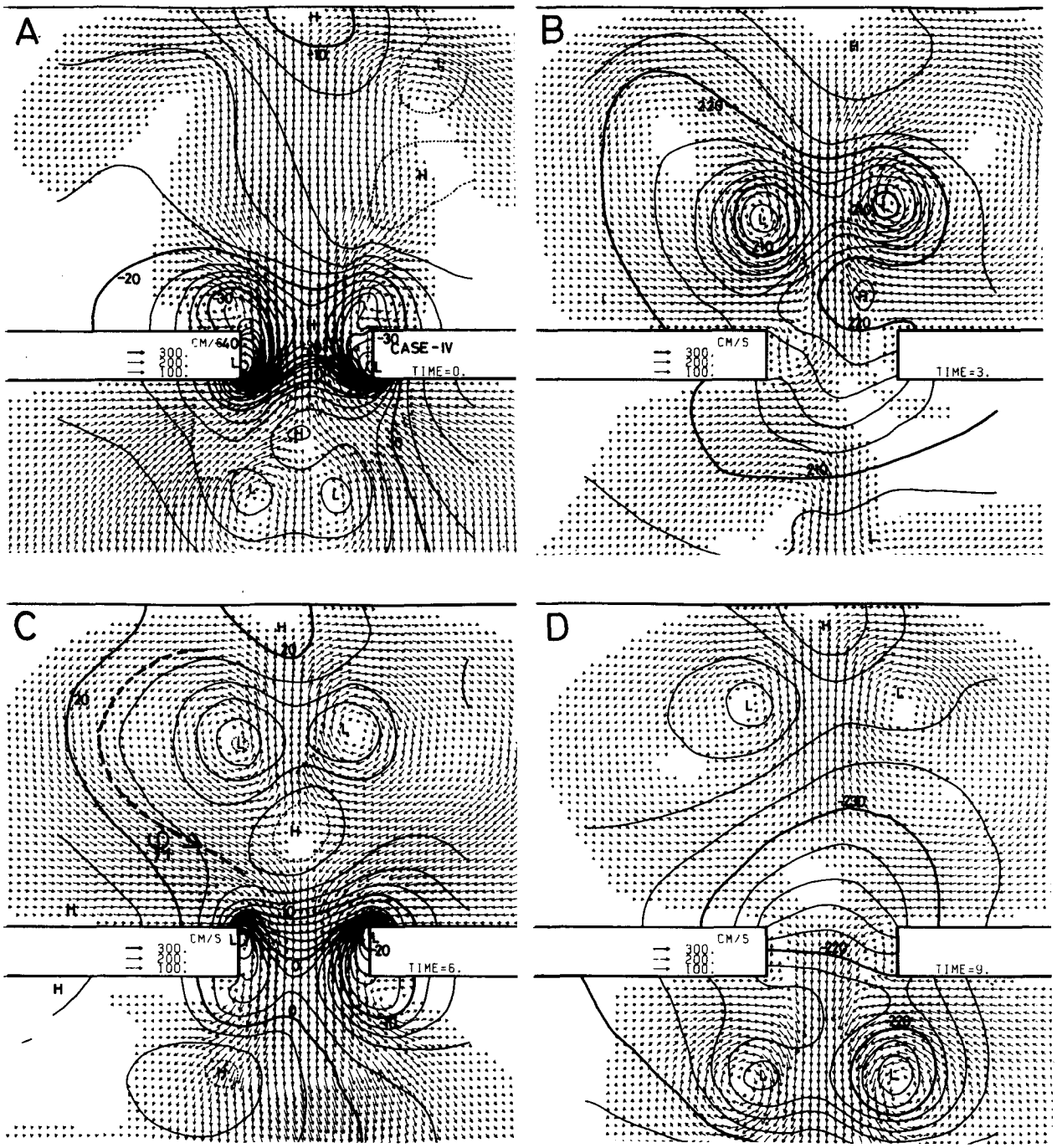

FIG. 5. Distribution of velocity vectors of tidal current in Case IV: (A) 0 h (the time of maximum flood current), (B) 3 h (just before the time of high-tide slack water), (C) 6 h (the time of maximum ebb current) and (D) 9 h (just before the time of low-tide slack water). Solid curves show the isobaric contour curves in intervals of 2 cm.

by the centrifugal force C and Coriolis force F, and it acts nearly normal to the left of the velocity vector (the right panel in Fig. 2B). Therefore, the water surface descends along the west coast of the strait. On the other hand, in the eastern area of the strait, the centrifugal force C is balanced by the pressure gradient force P and Coriolis force F, and therefore the water surface along the east coast of the strait is depressed. It can be seen that the low pressure area is mainly located around the cape of the peninsula and that the depression in the right-side area of the strait is smaller than that in the left-side area in the flood

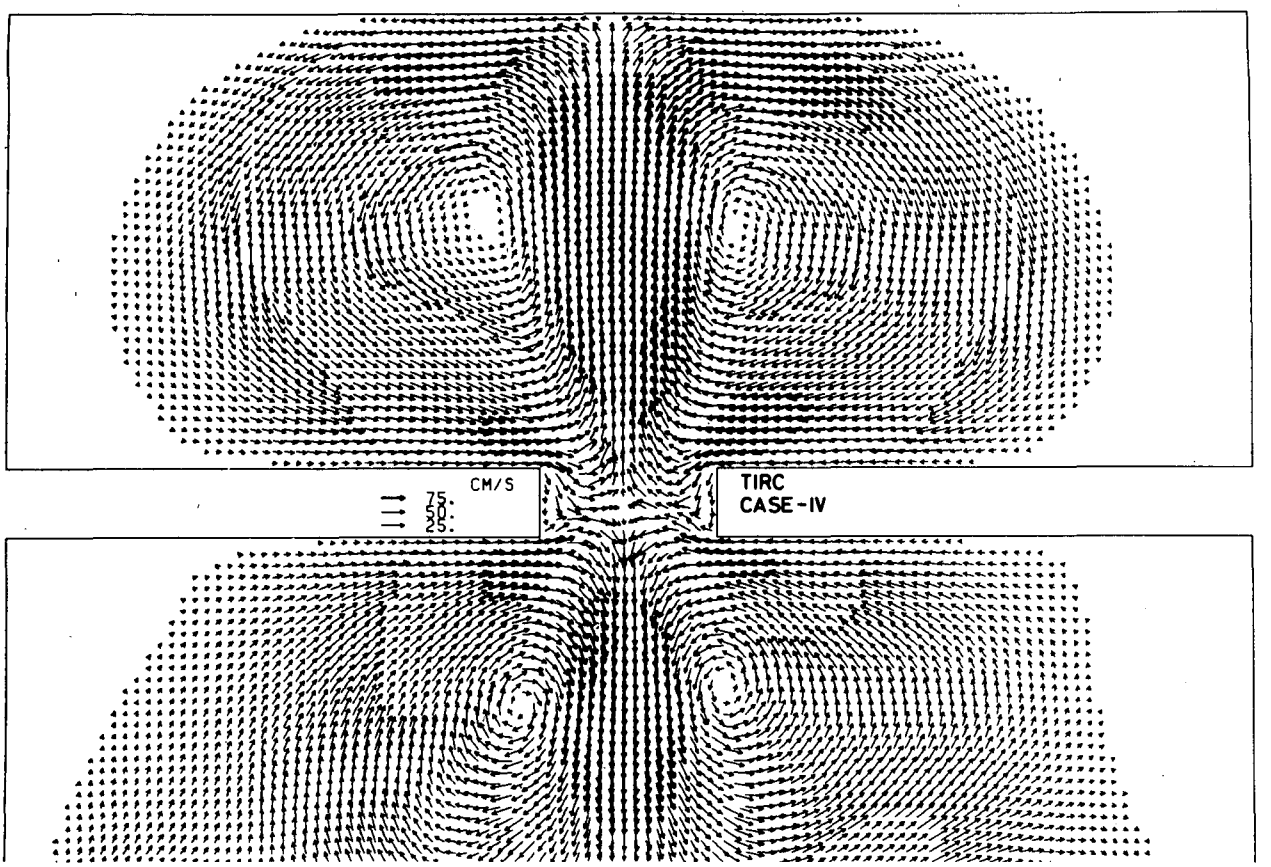

FIG. 6. Distribution of velocity vectors of TIRC in Case IV.

tide. The water surface in a low pressure area in the inner basin descends to a minimum level about the time of maximum flood current, and then water is driven by the pressure gradient force and starts flowing along the coast of the low pressure area toward the strait (the arrow in the right panel of Fig. 2C). Finally, the low pressure area increases in size and becomes a closed circulation as shown in Fig. 2E.

In Case I, the circulations in the inner basin disappear soon after the beginning of the ebb tide; two

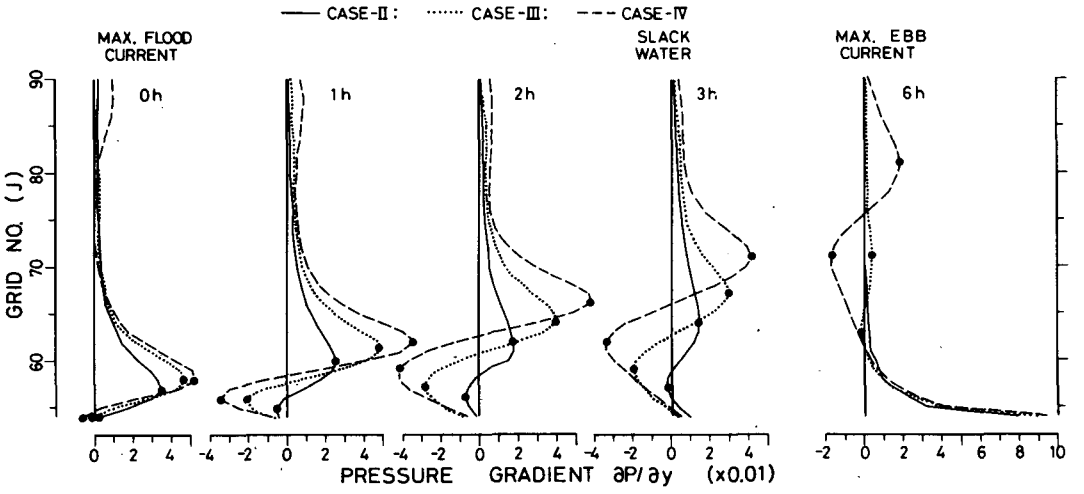

FIG. 7. Time change of distribution of pressure gradient $\partial P/\partial y$ along dashed line A in Fig. 8.

new circulations are generated in the outer basin at about the time of maximum ebb current and become eddies during the ebb tide. The process of generation, growth and decay of the tide-induced transient eddies is repeated near the narrow strait during every tidal cycle.

5. Lifetime of a tide-induced transient eddy "TITE"

We carried out three more calculations (Cases II, III and IV) to understand on what the lifetime of a transient eddy depends. Parameters of these three cases are tabulated in Table 1. In each of these cases, four transient eddies are also induced near the strait. The loci of the transient eddies are shown in Fig. 4, where a dot indicates the location of an eddy's center at every lunar hour. The transient eddies in the inner basin are present for ~4, 7 and 10 lunar hours in Cases II, III and IV, respectively.

The time changes of distribution of velocity vectors of tidal current in Case II are similar to those in Case I, and those in Case III are similar to those in Case IV. Next we will look at the time change of spatial distributions of velocity vectors and that of water surface elevation (in intervals of 2 cm) in Case IV. In Fig. 5, we find that the transient eddies are distinguished by the closed circular isobars. The flow patterns of tidal current in Case IV (Figs. 5A, C) are similar to those in the hydraulic model basin of Yanagi (1976, see Figs. 2 and 3 in his paper). Figure 6 illustrates the velocity vectors of so-called TIRC in Case IV.

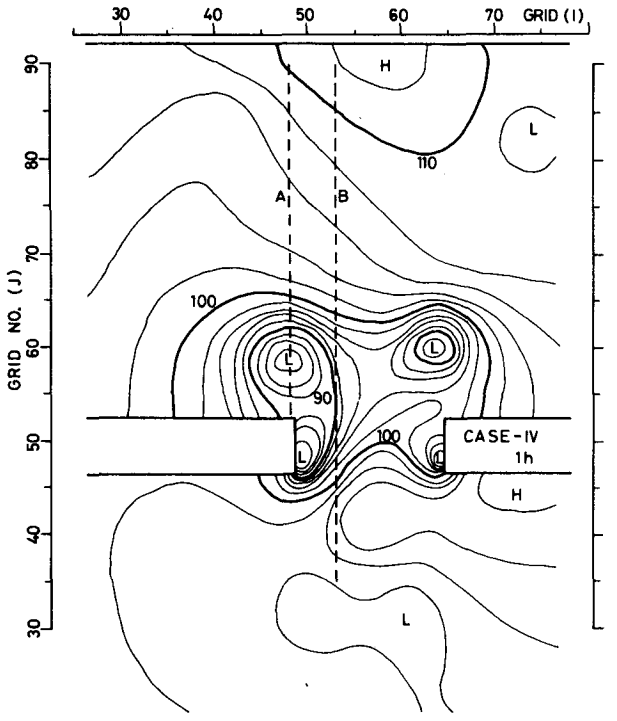

FIG. 8. Dashed lines A and B. Solid curves show the isobaric contour curves in intervals of 2 cm at 1 h in Case IV.

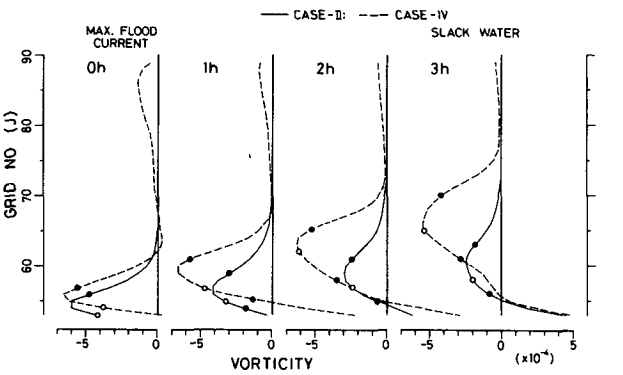

FIG. 9. Time change of distribution of vorticity ζ along dashed line A in Fig. 8 for Case II (solid line) and Case IV (dashed line).

Now we turn our attention to the left eddy in the inner basin of Cases II, III and IV to understand what the lifetime of TITE depends on, because these three cases are different only in the values of parameter γ_b^2 of the bottom friction. Figure 7 depicts the time change of the distribution of $\partial P/\partial y$ along broken line A in Fig. 8, which traverses the left transient eddy in the inner basin. In Fig. 7, a solid dot indicates the position of a maximum or a minimum value of $\partial P/\partial y$ around the eddy, and thus the area between these two solid dots represents the main part of the eddy. Figure 9 shows the distribution of vorticity $\zeta = \partial U/\partial y - \partial V/\partial x$ along broken line A in Fig. 8. Figures 7 and 9 demonstrate that the pressure gradient $\partial P/\partial y$ (water surface depression) and the vorticity ζ of the eddy in Case IV are larger than those in Case II. These phenomena are attributed to the fact that the velocity of the flood current flowing through the strait in Case IV is about 10% larger than that in Case II because the energy dissipation in Case IV is much smaller than that in Case II.

Fig. 10 shows the time change of the distribution of $\partial P/\partial y$ along the broken line B in Fig. 8. The distributions of $\partial P/\partial y$ just before the time of high-tide slack water (t = 3 h) reveal that $\partial P/\partial y$ in the strait is the largest in Case II (the strait is shown by the double-ended arrow symbol in Fig. 10), but on the other hand, $\partial P/\partial y$ in the eddy area is larger than that in the strait in Case III or IV. In Case II, the flows associated with the undulations of the pressure gradient in the inner basin are weaker than the ebbing flow in the strait, and the undulations are easily swept away by the ebbing tidal flow. In Cases III and IV, the ebbing flow is temporarily weak after the beginning of ebb tide, and cannot overcome the transient eddy. Moreover, at the time of maximum flood current, water has flowed along the south coast of the inner basin toward the strait as if the ebb tide had

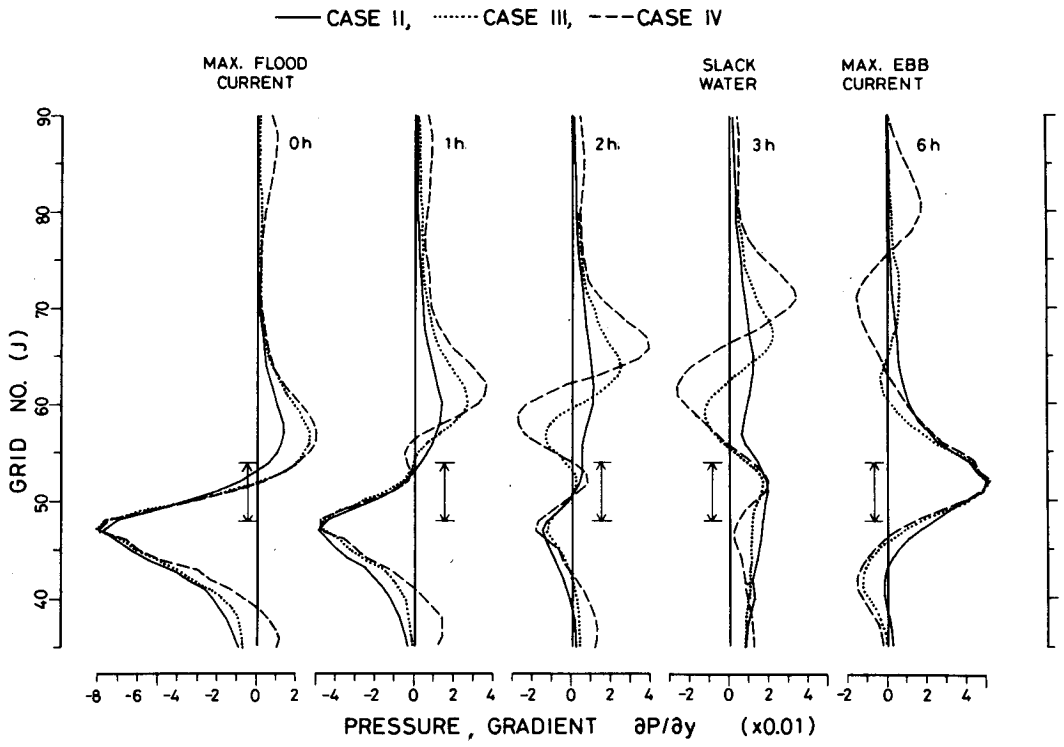

FIG. 10. Time change of distribution of pressure gradient $\partial P/\partial y$ along dashed line B in Fig. 8. The strait is shown by vertical double-ended arrow.

already begun at three lunar hours before the time of the high-tide slack water, and the speed is great when the transient eddy is dominant. Therefore, the major part of the ebbing tidal flow starts running along the south coast of the inner basin toward the outer basin through the strait, and during the ebb tide it runs along the curve ψ_1 in Fig. 5C. The centrifugal force C on the curve ψ_1 acts to maintain the transient eddy; the eddy moves toward the inner part of the basin because of the relation of continuity of water mass. Therefore, both the flood and the ebb tides are responsible for maintaining the eddy.

Why don't the transient eddies in Cases I and II become as large as the one in Case IV? The answer to this question is presented in Figs. 11 and 12. Fig. 11 shows the distribution of the vorticity dissipation

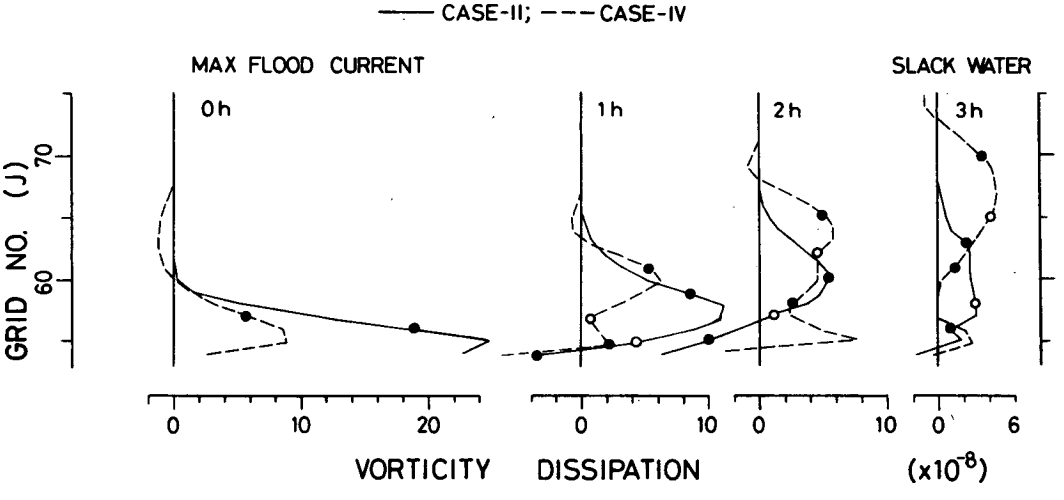

FIG. 11. Time change of distribution of vorticity dissipation V_D along dashed line A in Fig. 8.

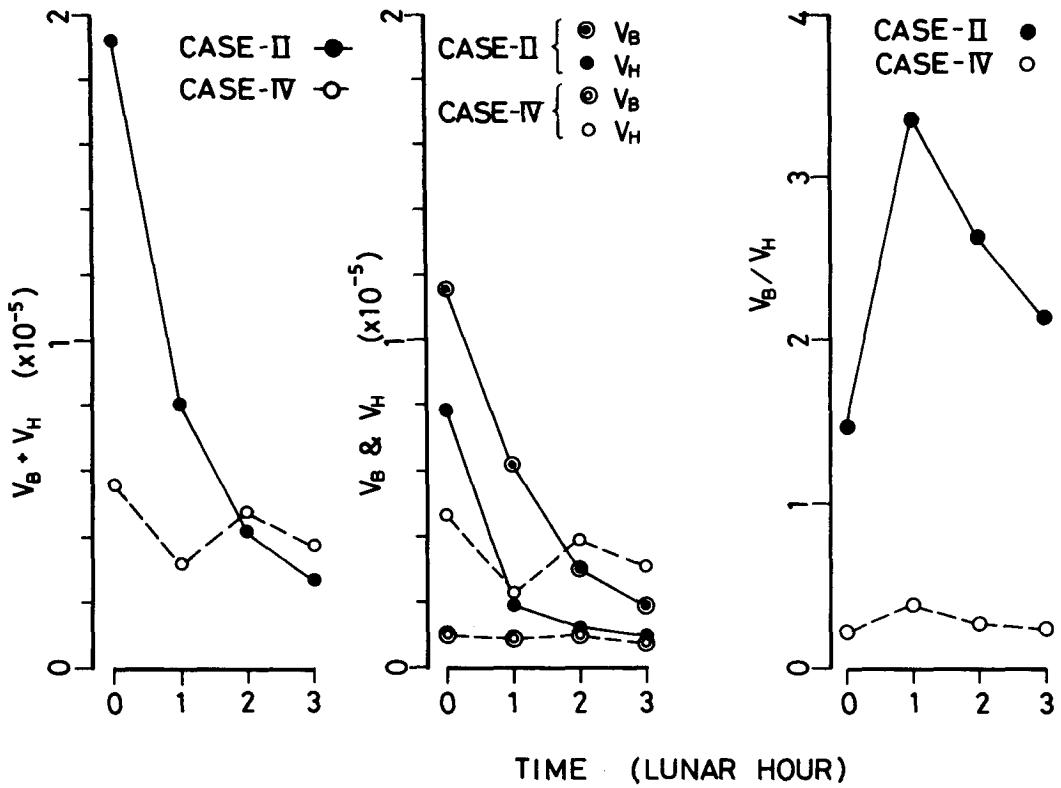

FIG. 12. Time change of vorticity dissipation $V_D = V_B + V_H$, V_B, V_H and the ratio of V_B/V_H in Cases II and IV.

V_D along dashed line A in Fig. 8. Vorticity dissipation V_D is given by

$$V_D = V_H + V_B$$
$$= \nu_H \nabla^2 \zeta + \gamma_b{}^2 \left[\frac{1}{H+\eta} \left(\frac{\partial V|\mathbf{U}|}{\partial x} - \frac{\partial U|\mathbf{U}|}{\partial y} \right) - \frac{|\mathbf{U}|}{H+\eta} \left(V \frac{\partial \eta}{\partial x} - U \frac{\partial \eta}{\partial y} \right) \right], \quad (8)$$

where V_H is the vorticity dissipation produced by the horizontal eddy viscosity and V_B is the vorticity dissipation produced by bottom friction. Figure 12 shows the time change of the mean value of vorticity dissipation in the main part of the transient eddy in the region between the two solid dots in Fig. 11. These figures show that the vorticity dissipation V_D of the eddy in Case II is very large for one or two hours after generation of the eddy, and the dissipation V_D reaches about three times that of Case IV. Panels B and C in Fig. 12 show that V_B in Case II is larger than V_H because of the large value of $\gamma_b{}^2$ and, on the other hand, V_H in Case IV is larger than V_B because of the large velocity shear near the transient eddy. Therefore the eddy in water of high viscosity (Cases I and II) cannot become as large as that in water of low viscosity, and the pressure undulation associated with a transient eddy is very small. On the other hand, a transient eddy in water of low viscosity becomes so large that the ebbing tidal flow cannot diminish it easily.

6. Discussion and conclusion

In advance of stating the concluding remarks, we need to discuss the Eulerian transport velocity defined as $\mathbf{U}_P = (H+\eta)\mathbf{U}/\langle H+\eta \rangle$. In this investigation, the value of constant depth H equals 30 m and η is less than 2 m. Therefore, η/H is less than 0.07 in the whole basin, and $\mathbf{U}_P \approx (1+\eta/H)\mathbf{U}$. Fig. 13 shows the distribution of the ratio

$$R_{CT} = \frac{|\mathbf{U}_{CT}|}{|\mathbf{U}_C|}$$

in Case I and Case IV. In this figure, a solid curve denotes the contour line of Eulerian residual current speed $|\mathbf{U}_C|$ normalized by a maximum speed $|\mathbf{U}_C|_{\max}$ of the Eulerian residual current. The dotted region enclosed by dashed lines denotes the area where the ratio R_{CT} is greater than 1.05 or less than 0.95. Fig.

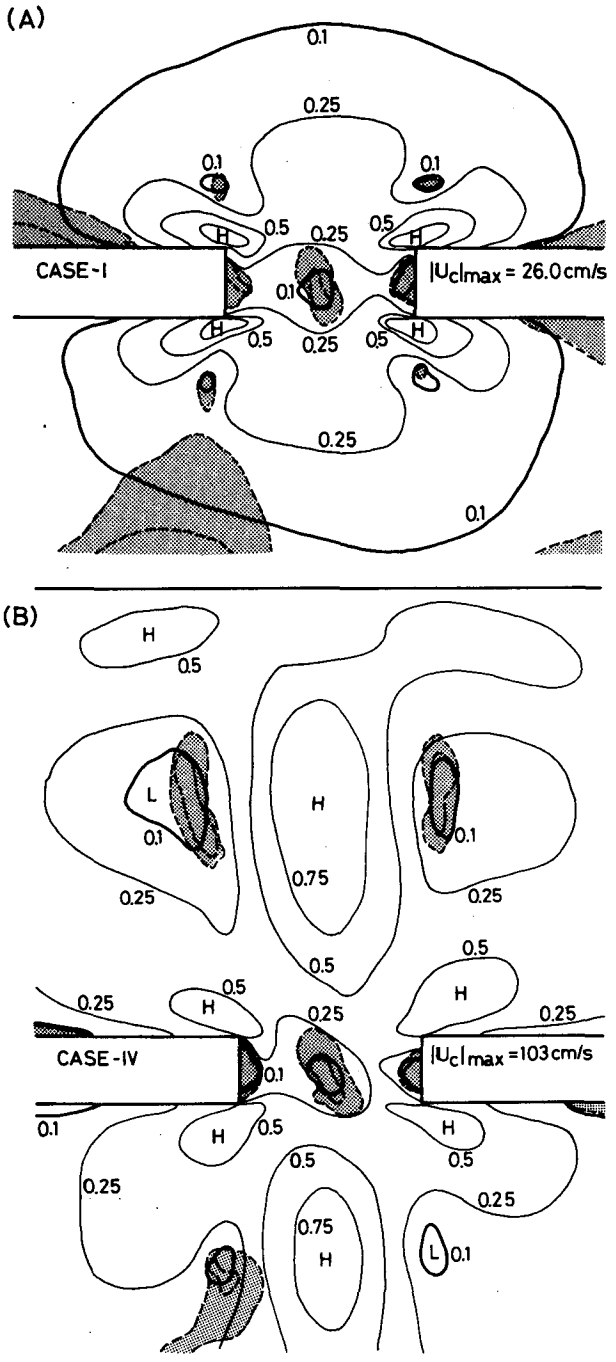

FIG. 13. Distribution of the ratio R_{CT} of Eulerian residual transport speed $|U_{CT}|$ to Eulerian residual current speed $|U_C|$, (A) Case I and (B) Case IV. Shaded region enclosed by dashed lines denotes the area where the ratio R_{CT} is >1.05 or R_{CT} < 0.95. Solid curves denote the contour of Eulerian residual current speed $|U_C|$ normalized by a maximum speed of Eulerian residual current.

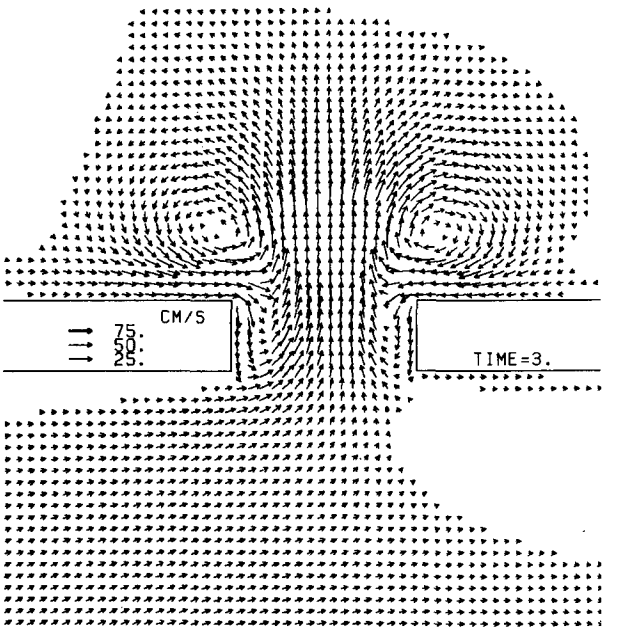

FIG. 14. Distribution of Eulerian transport velocity vectors in Case I at a time of high-tide slack water.

13 shows that the dotted area agrees with the region of weak residual current speed $|U_C|$, and that Eulerian residual transport velocity differs by only two or three percent from the Eulerian residual velocity in the area of significant speed of the Eulerian residual current. Fig. 14 shows the distribution of Eulerian-transport-velocity vectors in Case I at a time of high-tide slack water and the figure corresponds to the distribution of the Eulerian residual velocity vectors shown in Fig. 2E. The figures are in good agreement, and no circulation is found in the outer basin. A similar relation between the Eulerian residual velocity and the Eulerian residual transport velocity holds true in other cases. Therefore, without losing generality, we have the following conclusion.

The eddies (tide-induced transient eddy, TITE) shown in Figs. 2 and 5 originate from the low-pressure area generated downstream behind a headland by the nonlinearity or the centrifugal force of the tidal current flowing with a large curvature through a narrow channel. The lifetime of TITE depends on the magnitude of vorticity and its dissipation. In an inner basin with large bottom friction, the eddy diminishes for a short time (one or two hours) after the generation, and the pressure gradient of the eddy is smaller than the pressure gradient of tidal flow in the strait at the time of high tide slack water. In this case, TITE is swept away by the ebbing tidal current which flows outward through the strait and soon disappears. On the other hand, in a basin with small bottom friction, the eddy remains strong at the time of onset of ebb tide, and the pressure gradient becomes larger than that of the ebb tide. Consequently, the gyre is maintained by the ebbing tidal current which runs round

the eddy toward the strait. In the latter case, vorticity dissipation caused by horizontal eddy viscosity is larger than that caused by bottom friction because of a large horizontal velocity shear near the eddy.

The Eulerian tide-induced residual current is only a mathematical representation of the tide-induced transient eddy TITE or the result of the averaging process of transient phenomena, and has no physical reality. Then, we should abandon the concept of tide-induced residual velocity.

Acknowledgments. The numerical calculations were performed on a FACOM M200 in the Data Processing Center of Kyoto University. Part of this study was supported by the Grant-in-Aid for Scientific Research in 1981 (56030031) from the Ministry of Education in Japan.

REFERENCES

Cheng, R. T., and V. Casulli, 1982: On Lagrangian residual currents with applications in south San Francisco Bay, California. *Water Resour. Res.*, **18,** 1652–1662.

Hansen, W., 1956: Theorie zur Errechnung des Wasserstandes und der Stromungen in Randmeeren nebst Anwendungen. *Tellus,* **8,** 287–300.

Leendertse, J. J., 1971: A water-quality simulation model for well-mixed estuaries and coastal seas. Rand Corporation, England, 156 pp.

Oonishi, Y., 1977: A numerical study on the tidal residual flow. *J. Oceanogr. Soc. Japan,* **32,** 199–208.

Tee, K. T., 1976: Tide-induced residual current, a 2-D nonlinear numerical tidal model. *J. Mar. Res.*, **34,** 603–628.

Yanagi, T., 1976: Fundamental study on the tidal residual circulation I. *J. Oceanogr. Soc. Japan,* **32,** 199–208.

——, 1978: Fundamental study on the tidal residual circulation II. *J. Oceanogr. Soc. Japan,* **34,** 67–72.

Zimmerman, J. T. F., 1979: On the Euler–Lagrange transformation and the Stokes drift in the presence of oscillatory and residual current. *Deep Sea Res.*, **26A,** 505–520.